Continuous-scan capability at SSRL and applications to X-ray diffraction

Chunlei Li,[a]* Andrew M. Kiss,[b] Douglas G. Van Campen,[b]* Alex Garachtchenko,[b] Yuriy Kolotovsky,[b] Kevin Stone,[b] Yahong Xu,[c] Wenjun Zhang[a,d] and Jeff Corbett[b]

[a]East China University of Science and Technology, Shanghai, People's Republic of China, [b]SLAC National Accelerator Laboratory, Menlo Park, CA, USA, [c]Donghua University, Shanghai, People's Republic of China, and [d]University of Saskatchewan, Saskatoon, Canada. *Correspondence e-mail: chunlei520@gmail.com, campen@slac.stanford.edu

Typical X-ray diffraction measurements are made by moving a detector to discrete positions in space and then measuring the signal at each stationary position. This step-scanning method can be time-consuming, and may induce vibrations in the measurement system when the motors are accelerated and decelerated at each position. Furthermore, diffraction information between the data points may be missed unless a fine step-scanning is used, which further increases the total measurement time. To utilize beam time efficiently, the motor acceleration and deceleration time should be minimized, and the signal-to-noise ratio should be maximized. To accomplish this, an integrated continuous-scan system was developed at the Stanford Synchrotron Radiation Lightsource (SSRL). The continuous-scan system uses an in-house integrated motor controller system and counter/timer electronics. *SPEC* software is used to control both the hardware and data acquisition systems. The time efficiency and repeatability of the continuous-scan system were tested using X-ray diffraction from a ZnO powder and compared with the step-scan technique. Advantages and limitations of the continuous-scan system and a demonstration of variable-velocity continuous scan are discussed.

1. Introduction

The step-scan measurement approach traditionally moves stepper motors to discrete positions, and collects the data while the detector is stationary. It is a simple and direct method of recording data and has been used for many X-ray diffraction (Lu *et al.*, 2001; Wang, 1994; Reibenspies, 1993; Uvarov & Popov, 2007), X-ray absorption (Paktunc *et al.*, 2003) and X-ray tomography applications (Toda *et al.*, 2011). With the step-scan method, however, there are several potential drawbacks:

(i) Finite motor acceleration/deceleration time is needed at each step. Typically, the step size may be as small as $0.001°$ for an X-ray diffraction experiment (Pecharsky & Zavalij, 2005), and the detector might be moved over as much as $50°$, so approximately 50000 data points must be acquired. As the detector is moved to each new position, additional time is needed per data point for the motor acceleration/deceleration process. The acceleration and deceleration time is 300 ms at Stanford Synchrotron Radiation Lightsource (SSRL) beamline 2-1 and it is 500 ms at beamline 7-2. For the case at beamline 7-2, an extra 6.94 h is needed to complete a $50°$ scan. The added time can be reduced if a larger step size is used but important diffraction peaks may be missed.

(ii) System vibrations can be introduced due to motor acceleration and deceleration at each position. These vibra-

tions can decrease the signal quality by blurring the peaks. To decrease the effect of the vibrations, a settling time can be introduced, which will allow for the system to come to rest, but increases the data collection time.
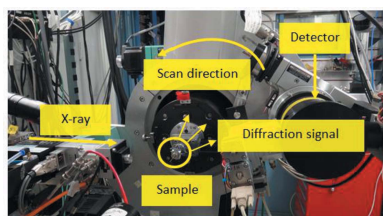
(iii) Often motor accuracy strategies are implemented, such as backlash correction, to improve detector position accuracy. These algorithms also require additional time to complete the step-scan process.

(iv) With longer scan time the probability of systematic instability increases. Variations can be caused by changes in temperature, beam intensity or sample degradation. Although some variations can be accounted for, it is best to minimize data collection time to reduce these effects.

Continuous-scan data acquisition by contrast offers an on-the-fly data measurement technique that avoids stopping motors to collect data at discrete positions and provides an alternative approach to bypass some of the drawbacks listed above. The SSRL continuous-scan system executes a pre-programmed motor trajectory sequence to smoothly move motors and synchronously record the signal at the detectors. One type of experiment that can readily benefit from the continuous-scan method is X-ray diffraction (XRD).

In an XRD experiment, to gain a sense for the location of diffraction peak positions and relative signal intensities, continuous-scan provides an efficient method to quickly scan peaks over a wide angular range. Results from a preliminary 'fast' scan can be used to adjust scan parameters for finer data acquisition to improve resolution of select diffraction peaks.

To date, continuous-scan systems have been developed at several laboratories using different commercially available motor controllers and data acquisition modules. At the Advanced Photon Source (APS) for instance, four kinds of motor controllers are in use: Newport MM4005, Newport XPS, Aerotech Ensemble and Pro-Dex MAXv. The APS system was developed using EPICS, where the memory of the Input/Output Controller was limited, so the resulting maximum number of trajectory segments was limited to 2000 (Rivers, 2014). At Diamond Light Source, a continuous-scan system was developed based on the Zebra data acquisition module and has been used for X-ray tomography (Cobb et al., 2013). At Synchrotron Soleil, a continuous-scan system has been used for X-ray microscopy and X-ray absorption with the whole system based on Tango and Python software (Joly et al., 2014; Medjoubi et al., 2013).

For the SSRL continuous-scan system, the maximum number of trajectory segments is 4096. The entire system is controlled at the top level using SPEC software. SPEC is popular for instrument control and data acquisition at many synchrotrons around the world. It has built-in macro capability to run continuous-scan trajectories using commercial motor controllers such as the Galil DMC4183 and the Newport XPS. The disadvantages of the SPEC continuous-scan macro are: (i) the lack of acceleration and deceleration segments before the start and after the end positions; (ii) a small delay between reading the signal data and motor position data; and (iii) a maximum scan time of 999 s. Therefore, it is desirable to develop a continuous-scan system to improve on the current capabilities.

This paper presents work to develop the continuous-scan capability at SSRL using integrated in-house motor controller and counter/timer electronics, commercially available data acquisition hardware and SPEC software to control the system. SSRL-developed hardware is based on programmable logic ICs with embedded microprocessor, DRAM controller and communication interfaces. It provides accurate timing (10 ns resolution), 32 counter channels (32-bit, 10^6 counts s^{-1} maximum rate), eight ADC channels (16-bit, 250 ksamples s^{-1} on each channel) with hardware support for averaging analog data over the data acquisition period, four motor channels (stepper motor, arbitrary motion profile), eight digital inputs and eight digital outputs (TTL level) that could be configured to synchronize scan with other instrumentation, data buffering, and 1 Gb Ethernet communication.

A major advantage of combining motion, data collection and timing hardware in one unit is the ability to accurately synchronize all functions, which may be difficult or impossible with separate pieces of equipment and software-controlled timing, leading to minimum dead-time between data points and maximum scan repeatability. In addition, programmable logic allows extended functionality of the same hardware for specific experiments by developing new logic configurations. Examples are photon absorber insertion control, collecting short data bursts at maximum rate for rapid scan tests, or laser timing control for pump–probe type experiments.

Preliminary test results using the SSRL continuous-scan system were reported by Li et al. (2015a). First applications included characterization of visible synchrotron radiation beam polarization as a function of vertical elevation angle at the SPEAR3 diagnostic beamline (Li et al., 2015b; Corbett et al., 2015). Here we present X-ray diffraction benchmark tests comparing continuous-scan results with step-scan measurements, as well as characterization of continuous-scan capabilities in terms of repeatability, time efficiency and accuracy as a function of scan velocity. These measurements were made using a zinc oxide (ZnO) powder sample at SSRL beamline 2-1. The continuous-scan method has the potential to benefit the synchrotron radiation user community in the future.

2. Continuous-scan method

The continuous-scan method was first tested using the XRD beamline at SSRL beamline 2-1. Here, the incoming X-rays diffract off the ZnO sample and were measured using a scintillation detector. During the scan process, the 2θ angle was changed as the motor moved the detector from the start to the end position. As illustrated in Fig. 1, the continuous-scan system contains two main subsystems: motor control and data acquisition.

During an XRD scan, the motor controller continuously moves the stepping motor, while the counter synchronously acquires the diffracted X-ray beam signal. SPEC software monitors the scan and handles the collected data from the
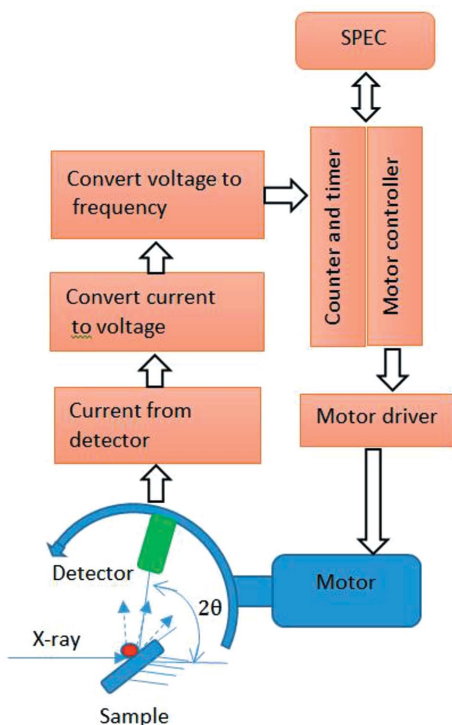
Figure 1
Schematic of the continuous-scan XRD system at SSRL beamline 2-1. The net diffraction angle between the incident X-ray beam and the detector is 2θ.

Table 1
Motion parameters for continuous scan.

Segment	Flag	Counting time	Velocity	Acceleration	Distance
Acceleration	0	t_0	v_0	a_0	d_0
Counting	1	t_1	v_1	a_1	d_1
...	...	...	...	...	...
n	1	t_n	v_n	a_n	d_n
Deceleration	$n+1$	0	t_{n+1}	v_{n+1}	a_{n+1}	d_{n+1}

controller and counter. The trajectory of the detector is defined in software by input parameters that specify the start position, end position, total number of data points and counting time for each segment of the trajectory.

Prior to initiating a data scan, the *SPEC* software macros automatically calculate operational parameters for each segment. These parameters include the velocity and acceleration for the detector on the 2θ arm. All parameters are verified internally to ensure they are within system limits before the scan is executed.

The three basic functional requirements (FR) for the continuous-scan system are:

FR-1: create and execute the movement trajectory according to the input parameters.

FR-2: acquire data during the detector movement process.

FR-3: synchronize the detector data acquisition with the motor motion.

The main principle for creating and executing a trajectory (FR-1) is to divide the whole trajectory into many discrete *segments* based on the total number of data points. Each segment in the trajectory will have specific settings so that it can maintain the correct motion path. These settings include the incoming velocity into the segment, constant acceleration for the segment, the displacement within that segment, and the total counting time for the segment. Appendix *A* provides a detailed explanation of how to calculate the parameters for each segment.

Specific values for each segment are calculated based on the scan settings provided by the user and calculated based on velocity profiles. A general equation, equation (1), was

formulated to be used with both constant and variable velocity scans. The velocity during the scan is simply based on the initial and final positions (s and f) and velocities (v_i and v_f), as well as an exponential factor (p) for scaling how the velocity changes with position,

$$v(2\theta) = v_i + (v_f - v_i)\left(\frac{|2\theta - s|}{|f - s|}\right)^p. \tag{1}$$

The other motion parameters in the trajectory are calculated to fulfill the velocity profile. For a scan with a constant velocity, the velocity terms will be the same and the acceleration for each segment will be set to zero. When the velocity is changing during a scan, the acceleration is calculated to best match the profile. By changing the value of the exponential factor, the shape of the velocity profile can be optimized for a given diffraction pattern to help maintain sufficient signal during the scan.

Once the segment motion parameters are calculated for a particular scan, they are compiled into a numerical array and sent to the motion controller shown in Table 1, each row representing one segment. The communication between the motion controller and *SPEC* is maintained continuously during the scan.

To fulfill FR-2 and collect the data during the scan, a count flag is utilized. The flag value will be either 1 or 0 to enable or disable data acquisition in each segment, respectively. For the acceleration and deceleration segments before the start position, the flag is 0, which means the counter/timer is idle. The flag is set to 1 for all segments between the start position and the end position, which indicates that the counter/timer will count voltage-to-frequency pulses during the specified segment when the detector is moving. When each segment is finished, the next segment will be executed automatically with a latency time of about 1 ns.

To fulfill FR-3 (synchronicity condition), the continuous-scan signal intensity is not recorded at a single, fixed position, but instead summed over the entire segment. As shown in Fig. 2, continuous-scan data collection begins half the distance before the center of a defined acquisition segment and terminates half the distance after the center. For example, the diffraction signal recorded with the central detector position at $2\theta = 30°$ over a segment $\Delta(2\theta) = 0.01°$ is the result of integrating photon counts between $29.995°$ and $30.005°$. As shown in Fig. 3, for a conventional step scan, the detector stops at each position and counts for a pre-defined signal integration time.
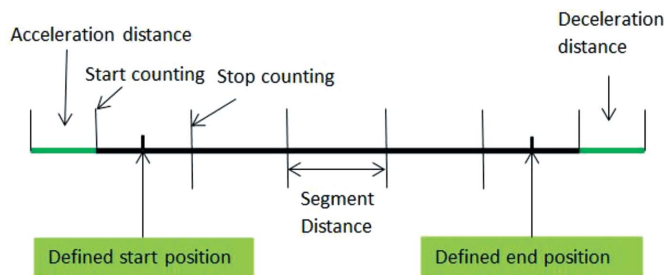
Figure 2
Synchronized continuous-scan motor position and collected data.
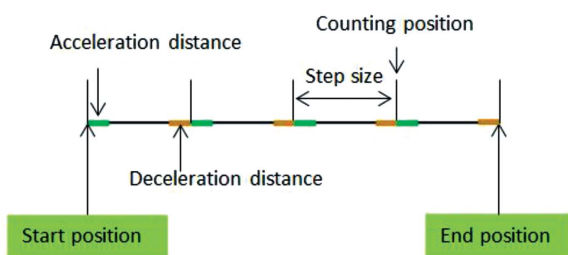
Figure 3
Step-scan motor position and data position.

Fig. 4 shows a schematic flow chart for the continuous-scan process. The motor first advances to the start position, and then accelerates to the specified velocity as calculated according to the time and distance parameters for the first segment. As soon as the detector accelerates to the start position, the detector begins to measure the signal. The data acquisition software then continuously integrates within each segment and records the resulting measurement values in memory. The measured counts are reset to zero before the next cycle begins. The process is repeated until the last scan segment has been executed. A similar flow chart for the step-scan method is shown in Fig. 5.

3. Experiment configuration

To test the continuous-scan system, a series of ZnO powder diffraction measurements were conducted at SSRL beamline 2-1. An annotated photograph of the experimental configuration is shown in Fig. 6. The ZnO powder sample was chosen because it has narrow diffraction peaks which span a wide range of scattering angles at 12.5 keV X-ray beam energy. The ZnO sample was first installed in a capillary, and then manually aligned to the X-ray beam using a five degrees-of-freedom stage.

The motor control subsystem uses an in-house motor controller, counter/timer chassis and stepping motor. The data acquisition is performed using a Bicron scintillation detector. *SPEC* software is used to interface with the motor controller and counter/timer. Detailed information about the software and hardware is shown in Table 2.

For the initial continuous-scan experiments, the SSRL in-house motor controller and counter/timer chassis were used.
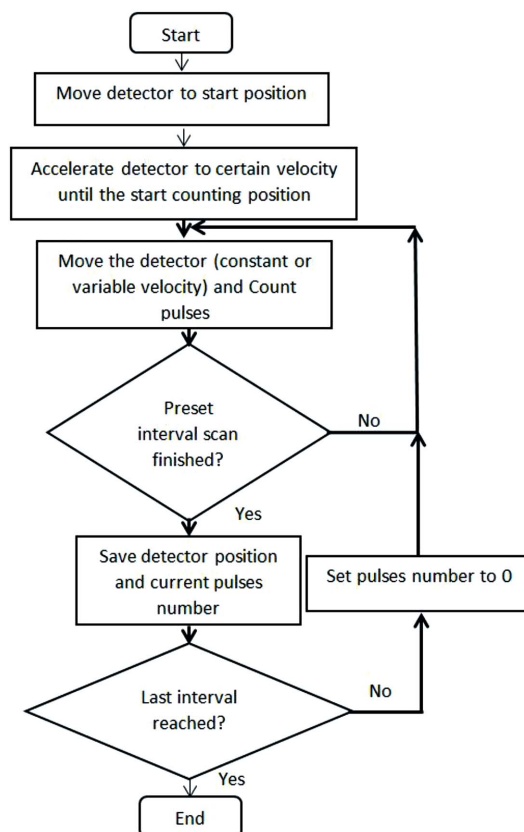
Figure 4
Flow chart for continuous scan.
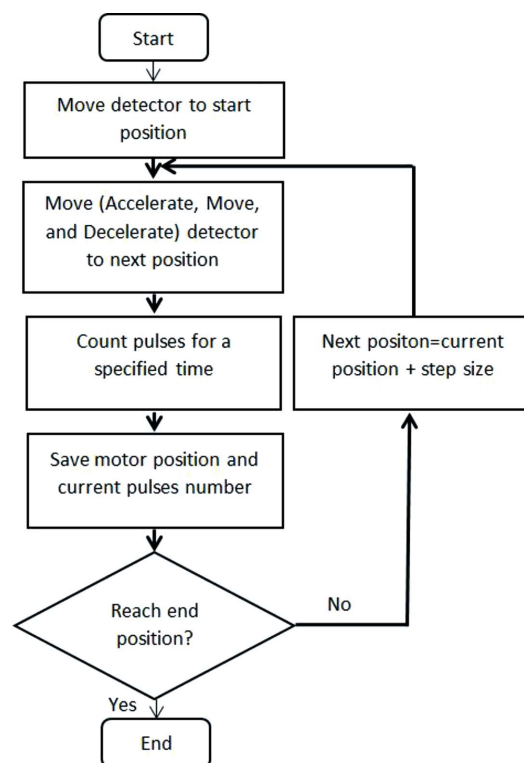
Figure 5
Flow chart for step scan.

Table 2
Components of the continuous-scan system.

Name	Model	Provider
SPEC	Version 6.02.08	Certified Scientific Software (USA)
In-house motor controller chassis	Firmware version 2.18, Hardware version 1.0b	SSRL (USA)
Vexta step motor	PK596BUA	Oriental Motor Co., LTD (USA)
Diffractometers	D8219 Rimsting	Huber (Germany)
Scintillation detector	1XMP.040B	Bicron (USA)
Current pre-amplifier	SRS570	Stanford Research System (USA)
Voltage to frequency converter	N101VTF	Nova R&D Inc (USA)
Counter/timer	PCI-6602	National Instruments (USA)
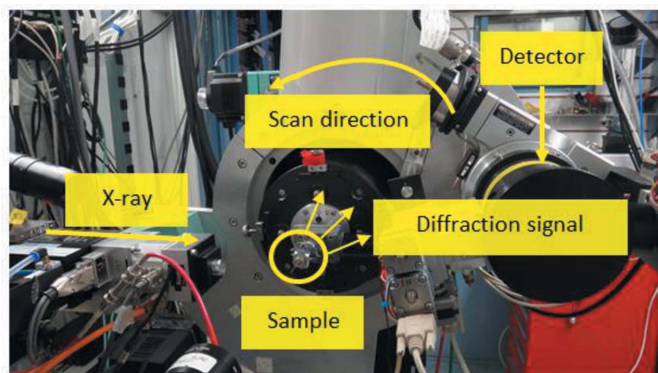
Figure 6
Configuration of the diffraction system at SSRL beamline 2-1.

The diffraction signal was first measured with the scintillation detector, then the signal was converted to a frequency using a voltage-to-frequency module, and finally the pulses were measured using the counter/timer in the SSRL-developed controller. For step-scan measurements, a Galil DMC-4183-NRE motor controller and National Instruments counter/timer were used to control the motor and count pulses, respectively. The parameters for the stepping motor for continuous-scan and step-scan measurements are shown in Table 3.

4. Results and discussion

In this section we discuss experimental results on the following topics:

(1) Data repeatability in the continuous-scan mode.
(2) Operation with different scan velocities and number of scan segments.
(3) Comparison with step-scan measurements.
(4) Time efficiency in continuous-scan mode.
(5) Continuous-scan mode with variable-velocity motor control.

4.1. Repeatability in continuous-scan mode

With conventional step-scan data acquisition, measurement accuracy depends on motor position reproducibility, dwell time and the corresponding signal-to-noise ratio of the detector. With continuous-scan data acquisition, two additional considerations come into play, namely data synchroni-

Table 3
Motor control parameters.

Parameter name	Value
Steps per degree	10000
Backlash (steps)	1000
Acceleration time (ms)	100
Steady-state rate (Hz)	20000
Base rate (Hz)	1

zation between motor position and detector readback, and overall speed of the continuous-scan system. Depending on the application, the accuracy of the peak position can be improved by using finer scan segments and similarly the accuracy of the peak area can be improved by integrating longer in each segment to improve detector counting statistics. A fundamental limit on peak position is determined by monochromater resolution and the fundamental limit on peak area determined by Poisson statistics.

4.1.1. Repeatability of continuous-scan data with constant velocity. To verify measurement repeatability, continuous-scan data were acquired between 20.0° and 20.5° to cover a single ZnO powder diffraction peak at 12.5 keV photon energy. It is important to collect sufficient data points in order to properly fit a diffraction peak with a Gaussian and it is commonly considered acceptable to collect 8 to 12 data points above the full width at half-maximum of the peak (Pecharsky & Zavalij, 2005). Experiments should be tailored to sufficiently meet this criterion. To test system repeatability, five back-to-back scans were performed each with 100 continuous-scan segments covering a 0.005° angular range with 1 s integration time per segment. Thus the scan velocity was $0.005°\,s^{-1}$ and the total scan time was 100 s. The raw data are plotted in Fig. 7 and results from numerical Gaussian curve fitting are shown in Table 4.

Comparing peak positions from Table 4, the fitted results indicate that the scans are consistent to the third decimal with a 95% confidence uncertainty of approximately 0.001° or 20% of a single measurement segment. The standard deviation in peak position over all five scans is only 0.0002°. Since each individual 2θ scan segment spanned 0.005°, the data indicate reliable electro-mechanical synchronization between the stepper motor and data acquisition system. Scan-to-scan numerical deviations are likely due to mechanical vibrations, digitization effects and/or detector noise which impacts the

Table 4
Fitted peak position, RMS width and integrated area for five 100-segment scans.

100-segment scan	Peak position (°)	RMS width (°)	Integrated area
Scan 1	20.2950 ± 0.0009	0.01382 ± 0.00091	40.61 ± 3.55
Scan 2	20.2950 ± 0.0010	0.01339 ± 0.00096	41.43 ± 3.94
Scan 3	20.2952 ± 0.0009	0.01333 ± 0.00091	42.53 ± 3.82
Scan 4	20.2954 ± 0.0009	0.01362 ± 0.00087	39.70 ± 3.34
Scan 5	20.2953 ± 0.0008	0.01368 ± 0.00086	40.62 ± 3.40

Table 5
Fitted peak position and line width σ for five different continuous-scan velocities.

Segment number	Velocity (° s^{-1})	Peak position (°)	RMS width (°)	Integrated area
100	0.0050	20.2953 ± 0.0008	0.01368 ± 0.00086	40.62 ± 3.40
150	0.0033	20.2962 ± 0.0007	0.01332 ± 0.00073	41.64 ± 2.99
201	0.0025	20.2965 ± 0.0005	0.01346 ± 0.00052	40.54 ± 2.10
300	0.0017	20.2958 ± 0.0004	0.01363 ± 0.00042	40.68 ± 1.67
500	0.0010	20.2958 ± 0.0004	0.01348 ± 0.00034	41.82 ± 1.39

Figure 7
Five ZnO diffraction peak scans centered near 20.3° with 0.005° angle interval per data point, 0.005° s^{-1} scan velocity and 100 data points per scan.
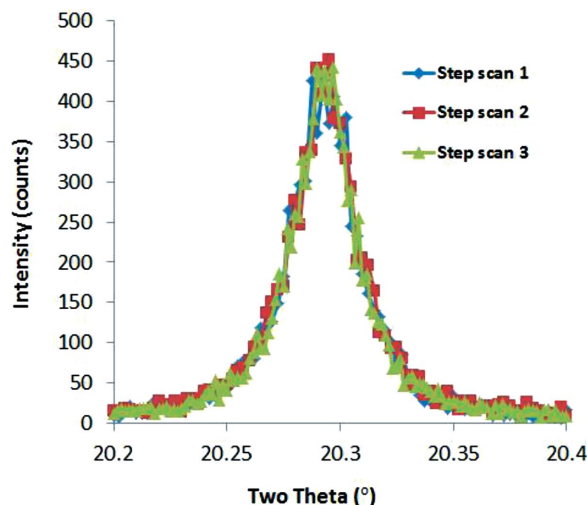
Figure 8
ZnO diffraction peak scans using five different scan velocities.

quality of the numerical curve fit. The reproducibility in the peak position of five sequential scans is less than the uncertainty in any single measurement demonstrating excellent synchronization in the data scans.

Integrated peak area is important in powder diffraction because it is used to determine atomic positions within the sample. Accurate measurement of peak intensities is therefore critical to determine crystal structure. For the reproducibility data reported in Table 4, a similar statistical argument can be made for the accuracy of the integrated area under each scan. In this case the standard deviation over the five measurements ($\sigma \simeq 1.1$) is less than the uncertainty of any single measurement. To within the measured uncertainty, the integrated areas are equivalent even though the total number of measurements within the FWHM was <8.

4.1.2. Comparison with different scan velocities. The flexibility to perform continuous scans at different velocities is important for rapid identification of diffraction peaks during preliminary sample screening runs. A comparison of continuous-scan measurements at different scan velocities was made, in this case by reducing the detector velocity from 0.005° s^{-1}, to 0.0033° s^{-1}, 0.0025° s^{-1}, 0.0017° s^{-1} and 0.001° s^{-1}. In each case, the corresponding number of scan segments was increased from 100, to 150, 201, 300, 500 with a constant integration time of 1 s per segment. The raw data for each scan are plotted in Fig. 8 with the Gaussian fit results listed in Table 5. Visually the reproducibility of the data scans appears accurate, but referring to Table 5 the center position is not

quite as accurate as the data reported above. Similar to §4.1.1, the number of data points above the full width at half-maximum is sufficient to properly fit the Gaussian curve through the data and differences in the peak location can be attributed to noise and spread based on the number of data points collected. As a result, we believe the SSRL continuous-scan system produces well synchronized diffraction peak scans over a range of different scan velocities. In §4.3 it is shown that significantly faster scan velocities result in loss of accuracy, as expected.

4.1.3. Comparison with conventional step-scan method. Since the conventional step-scan method has been widely validated, it was used to benchmark the continuous-scan system. The same 20.3° ZnO peak was scanned using the step-scan method. Fig. 9 shows the resulting data for three back-to-back scans with 100 step-scan segments. The counting time for each segment was 0.5 s. As expected, the diffraction peak scans again overlap well with the fitted peak positions and line widths shown in Table 6. The standard deviation for the peak positions across all three step scans is 2.00×10^{-4} deg corresponding to two motor pulses. The variation of the peak position is 2% of the segment distance. The standard deviation of the peak area is 0.2266 or 1.6% of the mean.

When comparing the repeatability of the continuous-scan data with the step-scan data shown in Table 7, it can be seen that the standard deviation of the continuous-scan data is very close to the step-scan data, in each case much less than the

Table 6
Peak position and area of step-scan result.

Step scan	Peak position (°)	Peak area
Scan 1	20.2929	14.6588
Scan 2	20.2933	14.7131
Scan 3	20.2931	14.2962

Table 7
Standard deviations of peak position and peak area.

D-p: standard deviation of peak position in pulses. D-a: standard deviation of peak area relative to the average area.

Scan type	D-p	D-a
Continuous scan with same scan velocity	2	2.6%
Continuous scan with different scan velocity	5	1.4%
Step scan	2	1.6%
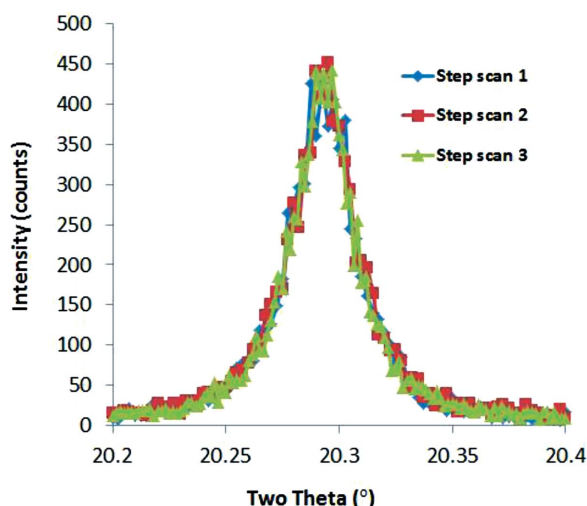
Figure 9
Diffraction peak data for three consecutive step scans.

Table 8
Peak position and peak area for step scans plotted in Fig. 10.

Peak number	Step scan 1		Step scan 2	
	Peak position	Peak area	Peak position	Peak area
1	20.2946	25.6157	20.2941	24.8435
2	21.9610	17.8113	21.9607	20.0650
3	23.1064	48.1314	23.1059	49.6517
4	30.0753	11.8467	30.0745	11.6998
5	35.5325	20.7442	35.5313	21.0250
6	39.2200	19.3155	39.2216	18.9267
7	41.2574	3.1710	41.2607	2.8768
8	42.1618	17.5138	42.1603	17.8583
9	42.8119	9.3719	42.8098	8.6261
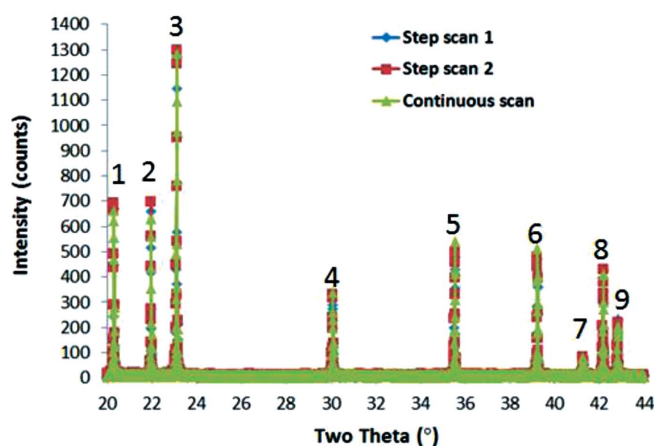
Figure 10
ZnO powder diffraction peaks at 12.5 keV measured by step scan and continuous scan for the same scan parameters.

scan segment distance. This implies that, under these scan conditions, the step-scan and continuous-scan approaches will provide similar quality data. When either of these scan methods are slowed or integrated over longer times, the data quality can be improved based on counting statistics.

4.2. Continuous-scan time efficiency

One significant advantage of the continuous-scan method lies in its time efficiency. To demonstrate the improved time efficiency of the continuous scan, a second comparison was conducted using both the step-scan and continuous-scan methods. The average of two long-time (about 1 h) step-scan measurements was used as a baseline. For the long-time step scan, the extra time for each segment was estimated based on a short scan from 20.0° to 20.5° with 200 step segments and 1 s count time at each step. The total scan time for the small-range scan was 248 s and the total counting time was 200 s; therefore the extra time for each segment was about 240 ms. As a result, 2903 segments were selected for a step scan from 20° to 44° with a 1 s counting time at each position; the total scan time was 3556 s. Next, a continuous scan was conducted with the

same range, same counting time and same segments. Only 2903.2 s was needed to finish the continuous scan.

To compare the scan measurements, the diffraction peak intensities for two step-scans and one continuous-scan over the 20° to 44° segment are shown in Fig. 10. Table 8 shows the step-scan peak positions and calculated areas for each peak based on Gaussian fitting. Table 9 shows the resulting average values from the two step-scans and the continuous-scan result. The maximum difference in peak position across the full scan relative to a single motor step size was only 15.73% (0.0013°). The maximum difference in calculated peak area was 6.68% except at peaks 2 and 7. At peak 2 the area under the curve differs between the two step-scan measurements; it is most likely because there were fewer than eight data points to fit the Gaussian curve as suggested by Pecharsky & Zavalij (2005). For peak 7 the diffraction intensity area was much smaller than all other peaks, so the magnitude was more easily influenced by noise in the measurement. Overall, it can be seen that the continuous scan has comparable performance with the step scan with the added benefit of 18.4% time savings for this set of conditions.

The continuous-scan efficiency depends strongly on the counting time of each position. When the counting time is much shorter than the moving time, there can be significant improvements with the continuous scan. However, if the counting time is much longer than the moving time, the time

Table 9
Comparison of continuous-scan and step-scan results.

Peak	Step scan		Continuous scan				Position error relative to step size (%)	Area error relative to step scan (%)
	Average positions	Average area	Peak position	Peak area	Difference of peak position	Difference of peak area		
1	20.2944	25.2296	20.2949	26.3856	0.0006	1.1560	6.65	4.58
2	21.9609	18.9382	21.9620	21.0548	0.0012	2.1167	13.91	11.18
3	23.1062	48.8916	23.1060	50.5121	−0.0002	1.6206	−1.81	3.31
4	30.0749	11.7733	30.0754	12.5594	0.0005	0.7862	6.05	6.68
5	35.5319	20.8846	35.5330	20.8770	0.0011	−0.0076	13.31	−0.04
6	39.2208	19.1211	39.2221	20.3050	0.0013	1.1839	15.72	6.19
7	41.2591	3.0239	41.2599	2.4424	0.0009	−0.5815	10.28	−19.23
8	42.1611	17.6861	42.1617	17.3873	0.0007	−0.2988	7.86	−1.69
9	42.8109	8.9990	42.8117	8.7770	0.0009	−0.2220	10.28	−2.47

efficiency benefits of the continuous scan are not as apparent. As a result, the continuous-scan method has enhanced benefit for high-brilliance X-ray sources due to the high photon flux and reduced counting time.

4.3. Continuous-scan performance with different segments or scan velocities

The effect of number of segments and scan velocity was tested for the continuous-scan method. For these tests, scan times of 60 min, 15 min and 4 min were performed. The scan range was from 20.0° to 44.0° and the counting time for each point was 1 s. The scan time was varied by changing the total number of data points, since each data point took 1 s. Therefore, the spatial resolution of the scan decreased with total scan time and varied from 0.0067° with the 60 min test up to 0.1000° for the 4 min test.

Fig. 11 shows the continuous-scan results with the same counting time at each position. The scan velocity increases when the segment distance is increased for a fixed amount of time. As a result, the peak values become smaller as there is less time to count pulses while at the peak position. From the 60 min scan result, the peak position slightly changes relative to the 4 min scan because the segment distance increases as the scan velocity increases for the same counting time; therefore, the resolution of peak position will decrease. As shown in Table 10, the peak position difference between the 60 min and 4 min continuous scan is 0.04° or 400 motor steps. Nevertheless, a visible peak is still noticeable in the 15 min fast scan. As a result of finding rough peak locations, further fine scans can be conducted based on the initial fast scan result. This fast continuous-scan mode of operation can be of great benefit to users who want to quickly

screen for individual diffraction peaks for a new sample. A similar fast scan with the step-scan technique would either require a high percentage of time lost to motor acceleration/deceleration or missed peaks altogether if the step size is too large.

4.4. Continuous-scan with variable motor velocity (acceleration/deceleration)

For many powder diffraction samples, the peak intensity at high-q scattering angles is weak (Da Silva *et al.*, 2007; Madsen & Hill, 1994). As a result, the signal-to-noise ratio decreases. In these cases it is desirable to increase the relative counting time at large angles to improve the signal-to-noise ratio. Variable-velocity continuous-scan profiles were investigated to satisfy this requirement. For a variable-velocity scan, a sequence-scan segment is defined in *SPEC* with the format
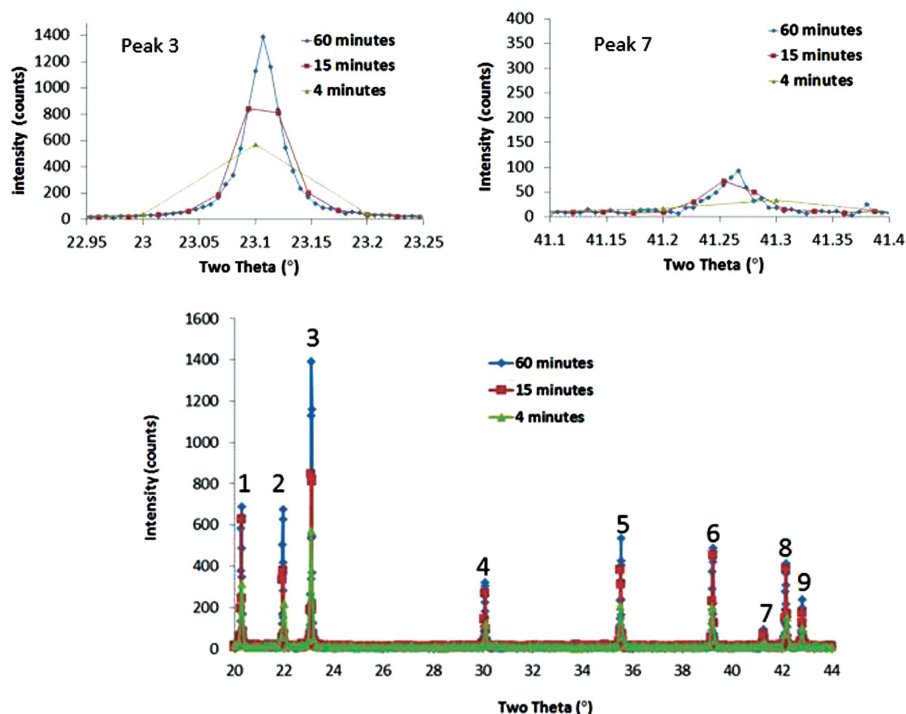
Figure 11
Continuous-scan result under different scan velocities.

Table 10
Peak position and peak intensity from two different scan segments or velocities.

Peak number	60 min		4 min		Peak position difference (P1 − P2)	Relative intensity difference (counts) (C1 − C2)
	Peak position (P1)	Relative intensity (counts) (C1)	Peak position (P2)	Relative intensity (counts) (C2)		
1	20.2933	686	20.3000	318	−0.0067	368
2	21.9600	677	22.0000	221	−0.04	456
3	23.1067	1390	23.1000	573	0.0067	817
4	30.0800	320	30.1000	120	−0.02	200
5	35.5333	536	35.5000	206	0.0333	330
6	39.2267	485	39.2000	205	0.0267	280
7	41.2667	94	41.3000	34	−0.0333	60
8	42.1600	414	42.2000	156	−0.04	258
9	42.8133	238	42.8000	101	0.0133	137

shown in Fig. 2 where the relation between the detector position and the count time is defined in equation (1). By defining the start and final counting time along with the exponential factor in equation (1), the velocity profile can maintain a constant signal-to-noise ratio. For example, when the signal is strong at low angles, and low at high angles, the exponential factor can be set to a value of ∼4 so that the velocity and counting time increase appropriately with angle. Future work will investigate variable-velocity continuous scans.

4.5. Continuous-scan limitations

Despite some of the time-saving advantages of the continuous-scan method, there are some limitations to the technique.

(i) The continuous-scan system requires the total scan range of the detector to be slightly larger than the measurement range due to the initial acceleration and final deceleration segments. This means that the detector cannot collect data up to the software or hardware limits because there will not be room for the acceleration and deceleration segment.

(ii) The maximum number of segments in the continuous-scan system is limited to 4096. For a total number of data points greater than 4096, the continuous-scan system was relaunched with a new scan after 4096 data points had been collected.

5. Conclusions

A continuous-scan system was tested for 2θ powder diffraction experiments at SSRL beamline 2-1 based on in-house SSRL motor control electronics. The X-ray diffraction experiment demonstrated accurate repeatability of continuous-scan measurements. The time efficiency of a continuous scan depends on the segment integration time, which can be significantly improved when the counting time is much less than the moving time. For samples where the peak positions are unknown, the continuous-scanning method is an efficient way to quickly record the distribution of diffraction peaks. Localized fine scans can then save valuable beam time. The continuous-scan method is particularly valuable when used with large high-inertia systems which require relatively long

times to start, stop and mechanically settle and for rapid-scan X-ray absorption spectra, particularly when the sample has a short lifetime in the X-ray beam. The new generations of high-brilliance X-ray sources will benefit from continuous-scan mode due to the high photon flux and therefore reduced counting time.

APPENDIX A
Scan segment parameter calculations

During a constant-velocity scan, the acceleration is zero throughout the data acquisition phase between the start and end points. During a variable-velocity scan the acceleration changes between segments as specified by the input parameters. Six parameters are needed to define each trajectory segment. They are the start position (s), the final position (f), the number of segments (n), the data acquisition time for the first segment (t_s), the data acquisition time for the last segment (t_f) and an exponential factor (p). The distance (d) of each piecewise trajectory segment is calculated from equation (2), and the velocity at the start and end positions can be calculated by equations (3) and (4), where v_{start} is the start position velocity and v_{end} is the end position velocity,

$$d = (f - s)/n, \tag{2}$$

$$v_{start} = d/t_s, \tag{3}$$

$$v_{end} = d/t_f. \tag{4}$$

For both constant-velocity and variable-velocity scans, the input velocity (v_{in}) and the output velocity (v_{out}) of each segment is calculated from equations (5) and (6), where N is the number of the current segment,

$$v_{in} = v_{start} + (v_{end} - v_{start}) \left(\frac{Nd}{|f - s|} \right)^p, \tag{5}$$

$$v_{out} = v_{start} + (v_{end} - v_{start}) \left[\frac{(N+1)d}{|f - s|} \right]^p. \tag{6}$$

The exponential factor, p, appearing in these equations dictates the tendency that the motor velocity decreases ($p > 1$) as the control segment is executed. The movement time, t, for each segment is calculated according to equations (7) and (8),

$$v_{ave} = (v_{in} + v_{out})/2, \tag{7}$$

$$t = d/v_{ave}. \tag{8}$$

To calculate the start (s_{start}) and end (s_{end}) positions for each segment, equations (9) and (10) are used, where s_{start} is the start position of each segment and s_{end} is the end position of each segment,

$$s_{start} = s + Nd - 0.5d, \tag{9}$$

$$s_{end} = s_{start} + d. \tag{10}$$

The acceleration segment is added before the start position and deceleration is added after the end position. The acceleration segment parameters can be calculated from equations (11)–(15), where d_{acc} is the acceleration distance, t_{acc} is the acceleration time, s_{start} is the start position of the acceleration segment, s_{end} is the end position of the acceleration segment, v_{in} is the input velocity of the acceleration segment and v_{out} is the output velocity of acceleration segment,

$$d_{acc} = 0.5v_{start}\, t_{acc}, \tag{11}$$

$$s_{start} = s - 0.5d - d_{acc}, \tag{12}$$

$$s_{end} = s - 0.5d, \tag{13}$$

$$v_{in} = 0, \tag{14}$$

$$v_{out} = v_{start}. \tag{15}$$

The deceleration segment parameters are calculated from equations (16)–(20), where d_{dec} is the deceleration distance, t_{dec} is equal to t_{acc} defined by the acceleration time in the *SPEC* configuration file, v_{in} is the input velocity of the deceleration segment and v_{out} is the output velocity of deceleration segment,

$$d_{dec} = 0.5v_{end}\, t_{dec}, \tag{16}$$

$$s_{start} = f + 0.5d, \tag{17}$$

$$s_{start} = f + 0.5d + d_{dec}, \tag{18}$$

$$v_{in} = v_{end}, \tag{19}$$

$$v_{out} = 0. \tag{20}$$

Acknowledgements

References

Cobb, T., Chernousko, Y. & Uzun, I. (2013). *Proceedings of the 14th International Conference on Accelerator and Large Experimental Physics Control Systems (ICALEPCS2013)*, San Francisco, USA, 6–11 October 2013, p. 736.

Corbett, J., Kiss, A. M., Li, C. L. & Boland, M. (2015). *Proceedings of the Sixth International Particle Accelerator Conference (IPAC'15)*, Richmond, VA, USA, 3–8 May 2015.

Da Silva, I. D., Gonzalez-Platas, J., Giacovazzo, C. & Altomare, A. (2007). *Z. Kristallogr.* **222**, 669–675.

Joly, L., Otero, E., Choueikani, F., Marteau, F., Chapuis, L. & Ohresser, P. (2014). *J. Synchrotron Rad.* **21**, 502–506.

Li, C. L. J., Corbett, J. & Mitsuhashi, T. (2015b). *Proceedings of the International Beam Instrumentation Conference (IBIC2015)*, Melbourne, Australia, 13–17 September 2015, pp. 364–368.

Li, C. L., Kiss, A. M. & Zhang, W. J. (2015a). *Proceedings of the Sixth International Particle Accelerator Conference (IPAC'15)*, Richmond, VA, USA, 3–8 May 2015, p. 1243.

Lu, L., Sahajwalla, V., Kong, C. & Harris, D. (2001). *Carbon*, **39**, 1821–1833.

Madsen, I. C. & Hill, R. J. (1994). *J. Appl. Cryst.* **27**, 385–392.

Medjoubi, K., Leclercq, N., Langlois, F., Buteau, A., Lé, S., Poirier, S., Mercère, P., Sforna, M. C., Kewish, C. M. & Somogyi, A. (2013). *J. Synchrotron Rad.* **20**, 293–299.

Paktunc, D., Foster, A. & Laflamme, G. (2003). *Environ. Sci. Technol.* **37**, 2067–2074.

Pecharsky, V. K. & Zavalij, P. Y. (2005). *Fundamentals of Power Diffraction and Structural Characterization of Materials.* New York: Springer.

Reibenspies, J. H. (1993). *J. Appl. Cryst.* **26**, 426–430.

Rivers, M. (2014). Trajectory scan note. Argonne National Laboratory, Chicago, USA.

Toda, H., Maire, E., Yamauchi, S., Tsuruta, H., Hiramatsu, T. & Kobayashi, M. (2011). *Acta Mater.* **59**, 1995–2008.

Uvarov, V. & Popov, I. (2007). *Mater. Charact.* **58**, 883–891.

Wang, H. (1994). *J. Appl. Cryst.* **27**, 716–722.